

Article

Removal of Amoxicillin Antibiotic from Polluted Water by a Magnetic Bionanocomposite Based on Carboxymethyl Tragacanth Gum-Grafted-Polyaniline

Seyedeh Soghra Mosavi ¹, Ehsan Nazarzadeh Zare ^{1,*} , Hossein Behniafar ¹ and Mahmood Tajbakhsh ²¹ School of Chemistry, Damghan University, Damghan 36716-45667, Iran² Department of Organic Chemistry, Faculty of Chemistry, University of Mazandaran, Babolsar 47416-13534, Iran

* Correspondence: ehsan.nazarzadehzare@gmail.com or e.nazarzadeh@du.ac.ir

Abstract: Removal of antibiotics from contaminated water is very important because of their harmful effects on the environment and living organisms. This study describes the preparation of a bionanocomposite of carboxymethyl tragacanth gum-grafted-polyaniline and $\gamma\text{Fe}_2\text{O}_3$ using an in situ copolymerization method as an effective adsorbent for *amoxicillin* antibiotic remediation from polluted water. The prepared materials were characterized by several analyses. The vibrating sample magnetometer and thermal gravimetric analysis showed that the carboxymethyl tragacanth gum-grafted-polyaniline@ $\gamma\text{Fe}_2\text{O}_3$ bionanocomposite has a magnetization saturation of 25 emu g^{-1} and thermal stability with a char yield of 34 wt%, respectively. The specific surface area of bionanocomposite of about 8.0794 m^2/g was obtained by a Brunauer–Emmett–Teller analysis. The maximum adsorption capacity (909.09 mg/g) of carboxymethyl tragacanth gum-grafted-polyaniline@ $\gamma\text{Fe}_2\text{O}_3$ was obtained at pH 7, an agitation time of 20 min, a bioadsorbent dose of 0.005 g, and *amoxicillin* initial concentration of 400 mg/L. The Freundlich isotherm and pseudo-second-order kinetic models were a better fit with the experimental data. The kinetic model showed that chemical adsorption is the main mechanism for the adsorption of *amoxicillin* on the bioadsorbent. In addition, the maximum adsorption capacity for *amoxicillin* compared to other reported adsorbents showed that the prepared bionanocomposite has a higher maximum adsorption capacity than other adsorbents. These results show that carboxymethyl tragacanth gum-grafted-polyaniline@ $\gamma\text{Fe}_2\text{O}_3$ would be a favorable bioadsorbent for the remediation of *amoxicillin* from contaminated water.

Keywords: *Amoxicillin* remediation; adsorption; magnetic bionanocomposite; carboxymethyl tragacanth gum; polyaniline; $\gamma\text{Fe}_2\text{O}_3$



Citation: Mosavi, S.S.; Zare, E.N.; Behniafar, H.; Tajbakhsh, M. Removal of *Amoxicillin* Antibiotic from Polluted Water by a Magnetic Bionanocomposite Based on Carboxymethyl Tragacanth Gum-Grafted-Polyaniline. *Water* **2023**, *15*, 202. <https://doi.org/10.3390/w15010202>

Academic Editor: Alejandro Gonzalez-Martinez

Received: 13 December 2022

Revised: 26 December 2022

Accepted: 31 December 2022

Published: 3 January 2023



Copyright: © 2023 by the authors. Licensee MDPI, Basel, Switzerland. This article is an open access article distributed under the terms and conditions of the Creative Commons Attribution (CC BY) license (<https://creativecommons.org/licenses/by/4.0/>).

1. Introduction

Pharmaceuticals, particularly antibiotics, represent a concerning new class of pollutants in the environment, not to mention their effects on human health with regard to several infectious illnesses [1,2]. Most of these chemicals are found in surface water at elevated amounts [3]. Their bioresistant character and ability to elude traditional sewage treatment procedures are strongly tied together. It harms the ecology by making bacteria resistant and interfering naturally with the growth, development, and movement of a variety of microorganisms [4]. One of the biggest obstacles to a sustainable water future is the presence of this material in the aquatic environment, particularly in arid nations where water recycling is crucial. As a result of their extensive use in both human and animal medications, antibiotics play a significant role in water contamination. They are employed to treat bacterial infections and are extremely resistant to being inactivated until they have completed their intended function, which causes their incomplete metabolism in the organism [5]. More than 90% of medications taken orally don't decompose, thus they become active compounds. Since antibiotics are highly soluble in water, conventional

treatment procedures cannot eliminate them, which poses a significant obstacle to their removal [6].

Amoxicillin is a commonly used antibiotic whose structure is based on a β -lactam antibiotic categorized as penicillin, which is the cause of its great bacterial resistance to many microorganisms [7]. Systemic, bacterial, and gastrointestinal illnesses are treated with *amoxicillin* in both human and veterinary medicine. It is widely recognized that *amoxicillin* is utilized in modern medicine, and its ecotoxicity contributes to the danger of medical wastewater. Due to the difficulty of breaking down this antibiotic, the residue is eliminated in the urine and feces. Consuming too much *amoxicillin* creates resistant bacteria because it accumulates in the body and feeds the organisms [8]. Consequently, an effective technique to remove it is essential before it is released into the aquatic environment.

The most common techniques for removing antibiotics include electrochemical degradation [9], Fenton oxidation process [10], UV radiation [11,12], ozonation [13], membrane filtration [14,15], photolysis [16], biological degradation [17], and adsorption [18]. The most appealing technology, nevertheless, is the adsorption process, which has a flexible and straightforward design, is simple to use, is inexpensive, and is highly effective [19,20]. The adsorbent used in industrial applications should be able to quickly absorb the target material and be ecologically benign [21]. The choice of an appropriate adsorbent for antibiotic elimination was the subject of several investigations. In order to effectively remove *amoxicillin* from water, a range of micro/nanostructures were deemed acceptable adsorbents, either as single phases or composites. Several works have reported the use of various adsorbents for the removal of *amoxicillin* from aqueous solutions. For example, a metal–organic framework (MIL-53(Al)) was prepared with a hydrothermal technique and used as an adsorbent for the removal of *amoxicillin* antibiotics from water [22]. It was reported that the adsorption capacity of MIL-53 is 758.5 mg g^{-1} in experimental conditions due to its high surface area. In another work, an adsorbent based on NH_4Cl -induced activated carbon was employed for the removal of *amoxicillin* from water [23]. It was expressed that the removal percentage of *amoxicillin* is above 99%, owing to the high specific surface area ($1029 \text{ m}^2/\text{g}$) of NH_4Cl -induced activated carbon. *Amoxicillin* removal from water was reported by an adsorbent based on activated carbon produced from pomegranate peel/iron nanoparticles [24]. The high removal percentage (97.9%) was obtained at a pH of 5 during a contact time of 30 min. A green magnetic adsorbent based on functional CoFe_2O_4 -modified biochar was used for *amoxicillin* removal from water. It was reported that the maximum adsorption capacity (99.99 mg/g) is obtained at a pH of 7 and at ambient temperature [25].

Of those, given their biodegradability, availability, reasonable cost, and minimal toxicity to biological systems, biopolymer-based composites have recently been used often as an ecologically friendly adsorbent to remove water contaminants. Natural polymer hydrogels were created using guar gum, karaya gum, xanthan gum, ghatti gum, and tragacanth gum. These natural polymers were capable of efficiently capturing pollutants in their three-dimensional (3D) network. As a result, the amount of interaction between contaminants and the hydrogel's surface functional groups is increased, improving adsorption effectiveness. They also have several industrial uses because of their capacity to hydrate in cold or hot water, either by stabilizing emulsion systems or by gel formation.

Tragacanth gum (TG), as a colorless and odorless natural polymer, is a highly complex heterogeneous anionic polysaccharide that forms from the stems and branches of *Astragalus gummier* and other Asian *Astragalus* species [26]. Within a few weeks, the exudate can be recovered after it has solidified into flakes or coils of ribbon [27]. Tragacanth gum is a substance that is found in Iran, India, Afghanistan, and Turkey. Neutral and anionic sugars, such as D-galacturonic acid, D-galactose, D-xylose, L-arabinose, L-fucose, and d-glucose are found in TG [26,28]. This natural polymer is widely used in the food industry, in medicine, and in cosmetics [29]. In addition, it is inexpensive, readily accessible, and has great solubility, strong thermal stability, and a long shelf life [30]. The existence of the hydroxyl- and carboxylic-acid-reactive functional groups in the TG can be used as chelating sites for the removal of pollutants from water. One method for improving the adsorption

capacity of natural polymers is copolymerization with functional monomers and adding inorganic fillers.

The aforementioned advantages can be strengthened by developing bionanocomposite materials that contain polyaniline and magnetic nanoparticles, such as $\gamma\text{Fe}_2\text{O}_3$. Consequently, in this study, a three-step oxidative polymerization procedure using ammonium persulfate oxidizer was used to create an antibacterial magnetic bionanocomposite based on carboxymethyl tragacanth gum-*grafted*-polyaniline, and then various aspects of it were examined. The bionanocomposite was subsequently applied for *amoxicillin* antibiotic removal from polluted water.

2. Materials and Methods

2.1. Materials and Instruments

Distilled aniline, ammonium persulfate, monochloroacetic acid, hydrochloric acid, iron(III) chloride hexahydrate, iron(II) chloride tetrahydrate, and other solvents were supplied by Merck Company (Darmstadt, Germany). Tragacanth gum (TG) with high-quality in translucent flakes was purchased from Rad Kimia-Garan Company (Tehran, Iran).

The chemical structure of prepared materials was studied by Fourier transform infrared (FTIR, Equinox 55, Bruker, Leipzig, Germany), elemental analysis (CHNSO, ECS 4010, NC technologies) and energy-dispersive X-ray (EDX, MIRA 3-XMU, Tescan, Kohoutovice, Brno-Kohoutovice Czech Republic). The crystallinity and morphology of the samples were assessed by X-ray diffraction (XRD, D8 Advance X-ray diffractometer, Bruker, Leipzig, Germany) and a field emission scanning electron microscope (FESEM, MIRA 3-XMU, Tescan, Kohoutovice, Brno-Kohoutovice Czech Republic). The specific surface area of the samples was studied by the Brunauer–Emmett–Teller (BET, Belsorp mini II, MicrotracBEL, Osaka, Japan) technique. The thermal behavior of the samples was investigated by thermogravimetric analysis (TGA, L81A1750, Linseis, Selb, Germany).

2.2. Preparation of Carboxymethyl Tragacanth Gum (CMT)

The carboxymethyl tragacanth gum (CMT) was synthesized according to our previous literature with slight modifications [31]. We fully dissolved 1 g of powdered tragacanth gum (TG) in a mixture of water/ethanol (85 mL/15 mL). Then, 1.2 g of NaOH in 10 mL of distilled water was added to the reaction mixture. The solution was kept at 50 °C for 30 min under a magnetic stirrer (Heidolph, Schwabach, Germany). Afterward, 1.3 g of monochloroacetic acid in 10 mL of distilled water was added to the reaction solution, and the final solution was stirred for 4 h at 50 °C. After cooling, the solution was poured into a double volume of ethanol or methanol. The resultant CMC sediment was separated using filter paper and dried at 40 °C (Figure 1).

2.3. Synthesis of $\gamma\text{Fe}_2\text{O}_3$

The co-precipitation technique was employed for the $\gamma\text{-Fe}_2\text{O}_3$ nanoparticles synthesis [32]. A solution of NaOH (1.0 M) was added to 100 mL of deionized water, and the reaction mixture was stirred magnetically for 15 min under an inert atmosphere. Afterward, a solution of iron(III) and iron(II) salts was dropped into the previous solution, and the final solution was kept under vigorous stirring at ambient temperature for 70 min. The resulting brown precipitate was separated and washed several times with distilled water and ethanol. Lastly, the precipitate was dried and the obtained powder was calcined at 300 °C for 2 h to gain the $\gamma\text{-Fe}_2\text{O}_3$ nanoparticles.

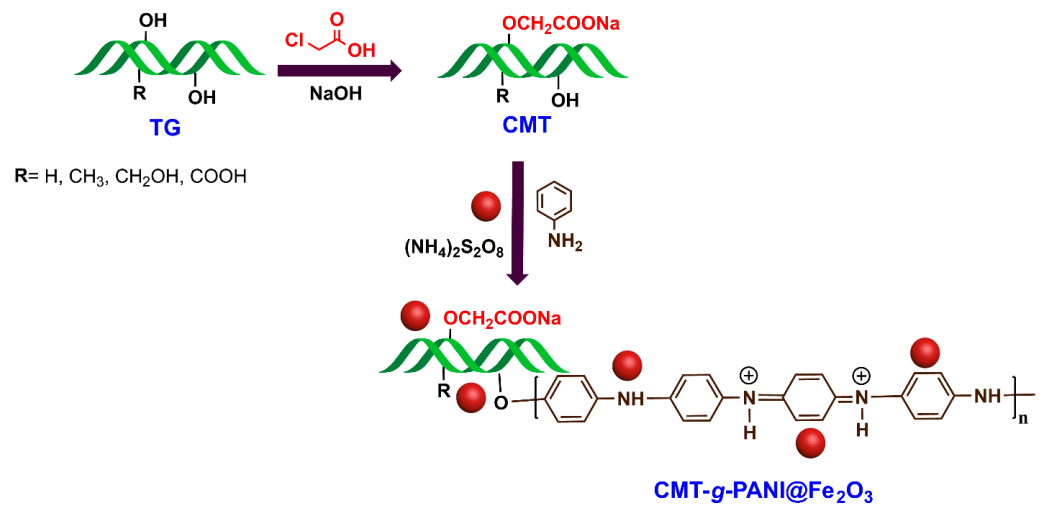


Figure 1. Schematic illustration of the preparation of carboxymethyl tragacanth gum (CMT) and carboxymethyl tragacanth gum-grafted-polyaniline@ γ -Fe₂O₃ (CMT-g-PANI@Fe₂O₃) bionanocomposite.

2.4. Preparation of Carboxymethyl Tragacanth Gum-Grafted-Polyaniline@ γ -Fe₂O₃

In a 250 mL round-bottom flask, 0.62 g of carboxymethyl tragacanth gum (CMT) was dissolved in 50 mL of distilled water. Then, 1.5 mL of HCl was added to the solution, and the flask was kept under N₂ gas at 0–5 °C. Subsequently, 10 wt% (an optimal amount) of γ -Fe₂O₃ nanoparticles were dispersed in 20 mL of distilled water for 30 min using an ultrasonic bath and then added to the above solution. After that, within 30 min, 3 g of ammonium persulfate in 10 mL of distilled water was added to the solution. The flask was then placed on a magnetic stirrer for 12 h under the aforementioned conditions after 1.25 mL of aniline monomer was added. The nanocomposite was separated by a magnet and rinsed with 10 mL of *N*-methyl pyrrolidone, water, and acetone before they were dried at 50 °C (Figure 1).

2.5. Adsorption Experiment

The carboxymethyl tragacanth gum-grafted-polyaniline@ γ -Fe₂O₃ (CMT-g-PANI@Fe₂O₃) bionanocomposite's ability to remove *amoxicillin* antibiotic from aqueous solutions was tested in a few different ways. The calibration curve of *amoxicillin* was prepared by defining the absorbance at 228 nm with a series of standard solutions (1–8 mg/L) achieved from reducing the stock solution at pH 7. Then, the *amoxicillin* initial or equilibrium concentrations were measured with the calibration curve [22].

Amoxicillin's initial concentration in an aqueous solution, solution pH, the amount of adsorbent, the agitation time, and other important parameters were all examined for their effects on adsorption capacity. The pH was changed from 4 to 9 using HCl (0.1 N) and NaOH (0.1 N). The optimal adsorption conditions were then investigated using a range of CMT-g-PANI@Fe₂O₃ biosorbent doses (0.005–0.025 g), contact periods (5–30 min), and initial *amoxicillin* concentrations (50–400 ppm). By comparing the outcomes of the experimental data with those predicted by the Freundlich and Langmuir models, the adsorption isotherms were also explored. To assess the adsorption kinetics, the pseudo-first-order and pseudo-second-order models were also applied. The experimental tests were carried out three times, and an average of the results was provided. A UV-visible spectrometer was used to assess the *amoxicillin* concentration. *Amoxicillin*'s capacity and adsorption efficiency onto CMT-g-PANI@Fe₂O₃ bionanocomposite were calculated using Equations (1) and (2), respectively [20].

$$R\% = \left(\frac{C_i - C_e}{C_i} \right) \times 100 \quad (1)$$

$$Q_e = \left(\frac{C_i - C_e}{m} \right) \times V \quad (2)$$

where C_i and C_e are the *amoxicillin* initial and the equilibrium concentrations in the solutions (mg/L), correspondingly. m is the weight (g) of CMT-g-PANI@Fe₂O₃ bionanocomposite and V is the solution volume (L).

2.6. Isotherm Study

Langmuir and Freundlich's isotherm models are used to evaluate the maximum adsorption capacity and equilibrium adsorption isotherms. The Langmuir isotherm model measured the single-layer adsorption of contaminants onto the adsorbent surface, whereas the Freundlich isotherm model measured the multilayer adsorption of pollutants on the adsorbent surface. The mathematical expression of Langmuir's (Equation (3)) and Freundlich's (Equation (4)) isotherm models are as follows [22,33]:

$$\frac{C_e}{Q_e} = \frac{1}{K_L Q_{\max}} + \frac{1}{Q_{\max}} C_e \quad (3)$$

$$\ln Q_e = \ln K_F + \frac{1}{n} \ln C_e \quad (4)$$

where, C_e , Q_e , and Q_{\max} are the equilibrium concentration (mg/L), the equilibrium, and maximum adsorption capacity (mg/g) correspondingly; K_L (L/mg) is the Langmuir constant calculated from the plot between C_e/Q_e and C_e ; K_F (L/mg) is the Freundlich constant calculated from the plot between $\ln Q_e$ and $\ln C_e$. n is a parameter to define the adsorption process favorability; once $n > 1$, the *amoxicillin* adsorption onto bioadsorbent is anticipated at high concentrations.

2.7. Kinetic Study

The famous kinetics models were used for studying the effect of time on the adsorption process. The mathematical expression of pseudo-first-order (PFO, Equation (5)) and pseudo-second-order (PSO, Equation (6)) models are shown as follows [22,33]:

$$\ln(Q_e - Q_t) = \ln Q_e - k_1 t \quad (5)$$

$$\frac{t}{Q_t} = \frac{1}{k_2 Q_e^2} + \frac{1}{Q_e} t \quad (6)$$

where Q_t (mg/g), and Q_e (mg/g) are the adsorption capacity at time t and equilibrium, correspondingly. k_1 (1/min) and k_2 (g/mg·min) are the rate constants of the PFO and PSO, correspondingly.

2.8. Desorption and Reusability

To examine the desorption and reusability of the CMT-g-PANI@Fe₂O₃ bionanocomposite, the *amoxicillin* adsorbed onto CMT-g-PANI@Fe₂O₃ bionanocomposite was floated in ethanol and stirred at ambient temperature for 1 h. After that, the bionanocomposite was separated by a magnet. The quantity of released *amoxicillin* in the elution medium was measured afterward employing a UV-visible spectrophotometer. The following equation was employed to obtain the desorption percentage.

$$\%D = \frac{A}{B} \times 100 \quad (7)$$

where A is the *amoxicillin* desorbed (mg) in the medium and B is the *amoxicillin* adsorbed (mg) on the CMT-g-PANI@Fe₂O₃ bionanocomposite.

3. Results and Discussion

Currently, the removal of antibiotic drugs from polluted water due to their destructive effect on humans and other living beings is very important. In this regard, we employed an antibacterial magnetic nanobiosorbent based on a carboxymethyl tragacanth gum-grafted-polyaniline and $\gamma\text{Fe}_2\text{O}_3$ nanoparticles (CMT-g-PANI@ Fe_2O_3) for the elimination of *amoxicillin* from contaminated water.

3.1. Nanobiosorbent Characterization

FTIR spectra are employed for studying the chemical structure of prepared materials and are shown in Figure 2A. In the FTIR spectrum of the TG, the absorption bands at 3470 cm^{-1} , 2934 cm^{-1} , and 1740 cm^{-1} are related to the stretching vibrations of the OH, $-\text{CH}$, and ester carbonyl groups, respectively [34,35]. In addition, the absorption band at 1604 cm^{-1} is due to the existence of the carboxylate anion of d-galacturonic acid. In the FTIR spectrum of the CMT, the absorption band at 1622 cm^{-1} is associated with the $-\text{COO}^-$ asymmetric vibrations which overlapped with the carbonyl groups of acidic and ester existing in the TG parts of the CMT [31,34]. Moreover, the absorption band that appeared at 1433 cm^{-1} is related to the bending vibrations of $-\text{CH}_2$. The FTIR spectrum of $\gamma\text{Fe}_2\text{O}_3$ nanoparticles displayed an absorption band at 550 cm^{-1} that was related to the stretching vibrations of Fe–O. Moreover, the bands at 1620 cm^{-1} and 3400 cm^{-1} were associated with the $-\text{OH}$ stretching vibrations on the surface of the $\gamma\text{Fe}_2\text{O}_3$ nanoparticles [36,37]. The FTIR spectrum of CMT-g-PANI displayed a broad absorption band at $\sim 3205\text{ cm}^{-1}$ and is related to the stretching vibrations of the N–H and OH of PANI and CMT, respectively. The absorption bands at 3050 cm^{-1} and 2949 cm^{-1} are attributed to aromatic and aliphatic C–H in the PANI and CMT, respectively. The two bands appearing at 622 cm^{-1} and 1470 cm^{-1} were related to the asymmetric vibrations of the $-\text{COO}^-$ and stretching vibration of the benzenoid ring, respectively [38]. The presence of characteristic absorption bands of CMT, PANI, and Fe_2O_3 in the FTIR spectrum of CMT-g-PANI@ Fe_2O_3 revealed that the bioadsorbent was synthesized.

The XRD analysis was employed for the investigation of the crystallinity nature of the samples as shown in Figure 2B. The XRD pattern of CMT showed an amorphous nature as compared to the XRD pattern of TG [31,39]. This crystallinity reduction may be related to the the $-\text{OH}$ group's replacement by the $-\text{COO}^-$ groups in the CMT [34]. A crystalline nature with diffraction peaks located at $2\theta = 23^\circ, 27^\circ, 34^\circ, 35^\circ, 41^\circ, 49^\circ, 53^\circ, 57^\circ, 62^\circ,$ and 63° was observed in the XRD pattern of Fe_2O_3 [39]. Synthesized Fe_2O_3 has an ordered cubic structure, which is consistent with JCPDS file no. 39-1346 [40]. XRD patterns comparison of CMT-g-PANI and CMT-g-PANI@ Fe_2O_3 showed that the crystallinity of CMT-g-PANI improved in the presence of Fe_2O_3 .

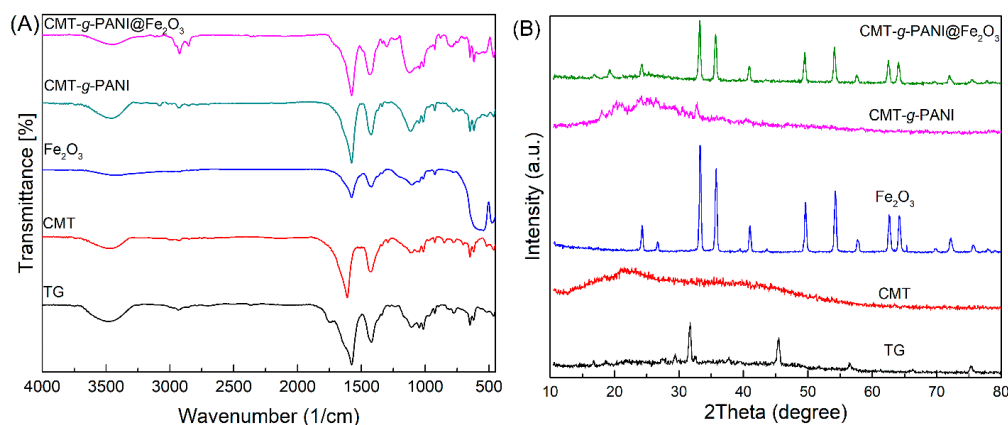


Figure 2. FTIR spectra (A) and XRD patterns (B) of TG, CMT, Fe_2O_3 , CMT-g-PANI, and CMT-g-PANI@ Fe_2O_3 .

The elemental analysis of TG, CMT, and CMT-g-PANI was performed, and the percentage mass contents of the elements are shown in Table 1. In CMT, the oxygen content reaches 66.27% as compared to TG which means that the substitution of $-\text{COO}^-$ was carried out in the TG, successfully. Correspondingly, in CMT-g-PANI, the oxygen content decreased to 47.71%. This could be related to the grafting reaction between CMT and PANI. Furthermore, the presence of nitrogen content of 8.03% in CMT-g-PANI is related to the PANI.

EDX examination was also applied for the chemical structure study of the prepared samples as shown in Figure 3A. The existence of C, O, Cl, and Na elements in the EDX spectrum of CMT confirmed the preparation of CMT and the substitution of $-\text{COONa}$ in the TG backbone. The existence of a tiny amount of Cl is related to chlorine removal from monochloroacetic acid due to the nucleophilic substitution reaction between the hydroxyl of TG and monochloroacetic acid. The presence of Fe and O elements in Fe_2O_3 and C, N, O, Cl, and Na elements in the CMT-g-PANI expressed that the Fe_2O_3 and CMT-g-PANI@ Fe_2O_3 were prepared. In addition, the presence of C, O, N, Fe, Cl, and Na in CMT-g-PANI@ Fe_2O_3 showed that the bionanocomposite was prepared successfully.

Table 1. Elemental analysis of TG, CMT, and CMT-g-PANI.

Sample	C	H	N	O
TG	42.19	5.71	-	52.1
CMT	29.66	4.07	-	66.27
CMT-g-PANI	39.88	4.38	8.03	47.71

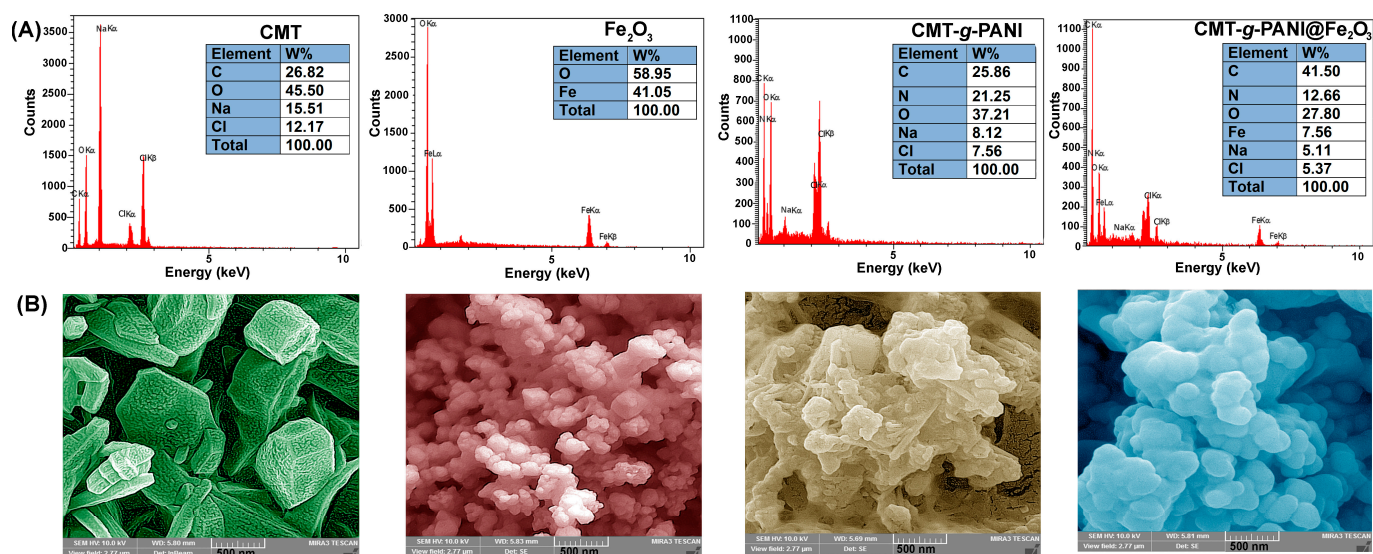


Figure 3. EDX spectra (A) and FESEM micrographs (B) of CMT, Fe_2O_3 , CMT-g-PANI, and CMT-g-PANI@ Fe_2O_3 .

Figure 3B shows the FESEM micrographs of CMT, Fe_2O_3 , CMT-g-PANI, and CMT-g-PANI@ Fe_2O_3 . The FESEM image of CMT shows polyhedral particles with microsize. It appears that the chemical modification of TG leads to the formation of polyhedral microparticles. The nano-spherical and amorphous structures were observed in the FESEM images of Fe_2O_3 and CMT-g-PANI. The presence of Fe_2O_3 nanoparticles lead to a granular structure in the FESEM image of CMT-g-PANI@ Fe_2O_3 .

VSM analysis was employed to evaluate of magnetic properties of Fe_2O_3 and CMT-g-PANI@ Fe_2O_3 as shown in Figure 4A. The magnetization saturation (M_s) values of Fe_2O_3 and CMT-g-PANI@ Fe_2O_3 were 70 emu g^{-1} and 25 emu g^{-1} , respectively, and showed

superparamagnetic properties for both. In addition, the M_s value of Fe_2O_3 decreased with the coating of Fe_2O_3 by CMT-g-PANI.

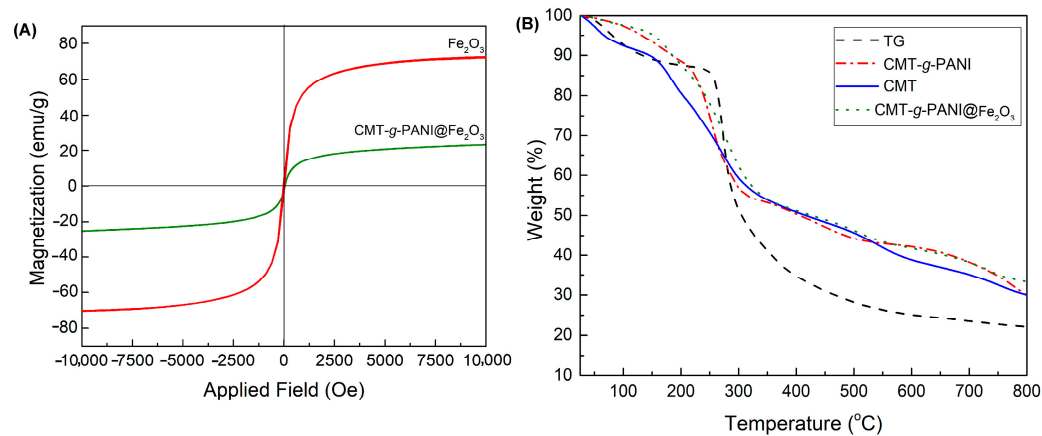


Figure 4. VSM curves of Fe_2O_3 , and CMT-g-PANI@ Fe_2O_3 (A) and TGA thermograms (B) of TG, CMT, CMT-g-PANI, and CMT-g-PANI@ Fe_2O_3 .

TG analysis was applied to study the thermal stability of prepared materials as seen in Figure 4B. The TGA thermogram of TG displays two steps of mass loss from 50 to 178 °C and from 200 to 580 °C. The first mass loss (10 wt%) was related to the removal of moisture absorbed in the TG, and the second mass loss (65 wt%) corresponded to the branched heterogeneous structure degradation of the TG [34,39]. The char yield of TG at 800 °C was 25 wt%. Four mass losses at 30–150 °C, 150–300 °C, 300–550 °C, and 550–780 °C were observed in the TGA thermogram of CMT. The first (10 wt%) and second (32 wt%) mass losses were related to the moisture evaporation and combination of the saccharide ring degradation, the C–O–C breaking, and the CO_2 elimination from the CMC, respectively [34,39]. The two latter mass losses were attributed to the CMT backbone breaking [39]. The char yield of CMC at 800 °C was 33 wt%. In the TGA thermogram of CMT-g-PANI, four mass losses were observed. The first mass loss (10 wt%) at 5–200 °C was caused by the evaporation of water and solvent entrapment in the copolymer chains [41]. The second mass loss (25 wt%) at 200–300 °C probably corresponded to the loss of hydrochloric acid, saccharide ring, and the CO_2 elimination from the CMT-g-PANI. The third mass loss (10 wt%) at 300–500 °C and the fourth mass loss (20 wt%) at 500–750 °C was ascribed to the breakdown of sugar units in the CMT structure and PANI, respectively. The char yield of CMT-g-PANI at 800 °C was 34 wt%. Compared with CMT-g-PANI, the thermogram of the CMT-g-PANI@ Fe_2O_3 showed good thermal stability owing to the existence of Fe_2O_3 nanoparticles in the CMT-g-PANI matrix.

Brunauer–Emmett–Teller (BET) analysis was applied to define the specific surface area of materials and evaluate the effect of the presence of Fe_2O_3 nanoparticles within the CMT-g-PANI matrix, as seen in Figure 5. The specific surface area ($a_{s,BET}$) values of CMT-g-PANI@ Fe_2O_3 and Fe_2O_3 were 8.0794 m^2/g and 2.8278 m^2/g , respectively. This confirms that the CMT-g-PANI@ Fe_2O_3 had better surface properties in terms of surface area and micropore area compared to Fe_2O_3 . Thus, the presence of Fe_2O_3 together with CMT-g-PANI led to an improvement in the $a_{s,BET}$ value of CMT-g-PANI@ Fe_2O_3 which could be effective in antibiotic adsorption by bioadsorbent.

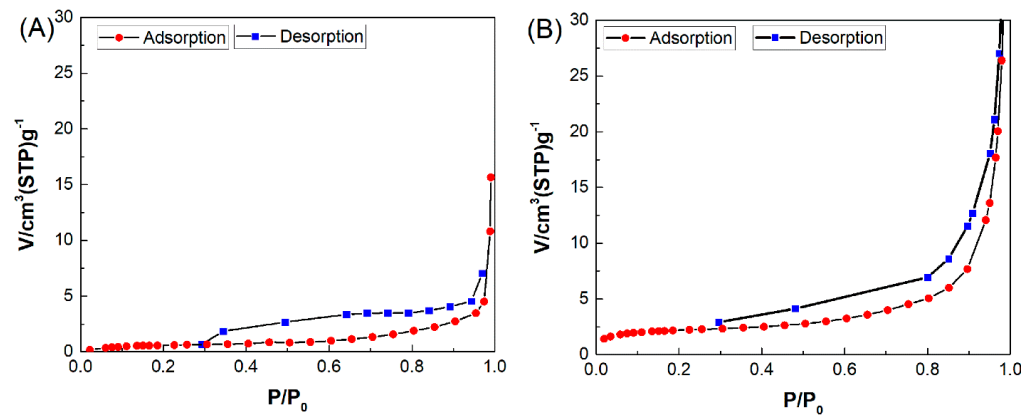


Figure 5. N_2 adsorption/desorption isotherms of Fe_2O_3 (A) and CMT-g-PANI@ Fe_2O_3 (B).

3.2. Optimization of Effective Parameters for Amoxicillin Adsorption

Solution pH: It is well known that the changes in the medium pH can directly affect the removal percentage of pollutants from an aqueous solution. In this regard, a solution pH range of 4–9 for finding the best pH for *amoxicillin* adsorption by the CMT-g-PANI@ Fe_2O_3 was examined (Figure 6A). Results revealed that by growing the pH values from 4 to 7, the Q_e increased from 54.18 mg/g to 65.39 mg/g and then decreased at high pH (8 and 9). At pH 7, *amoxicillin* antibiotic occurs as zwitterions, while at pH 4 and 5, it performs in cationic species, and at pH 8 and 9, it appears in anionic species. Thus, *amoxicillin* removal was efficient under pH 7 (neutral). The hydroxyl, carboxyl, and amine groups in the copolymer together with a high surface-to-volume ratio of Fe_2O_3 in the CMT-g-PANI@ Fe_2O_3 adsorbent lead to the rapid diffusion of *amoxicillin* molecules into the adsorbent and interaction with its functional groups for efficient *amoxicillin*.

Amount of biosorbent: Adsorption examinations were carried out with changing quantities (0.005–0.025 g) of the CMT-g-PANI@ Fe_2O_3 at pH 7 (optimal) to investigate the association between the adsorbent amount and its adsorption capability for *amoxicillin*. According to Figure 6B, the Q_e decreased from 189.73 to 34.50 mg/g as the adsorbent amount increased from 0.005 g to 0.025 g. At a lower adsorbent amount, the higher the amount of *amoxicillin* adsorbed by the CMT-g-PANI@ Fe_2O_3 . The optimal quantity of CMT-g-PANI@ Fe_2O_3 for subsequent examinations was found to be 0.005 g.

Agitation time: The agitation time effect on the Q_e of the CMT-g-PANI@ Fe_2O_3 adsorbent for the removal of *amoxicillin* was examined (Figure 6C). Results showed that the Q_e increased up to 195.49 mg/g by increasing the agitation time from 5 to 20 min at pH 7 with an adsorbent dose of 0.005 g (optimal). Furthermore, the Q_e decreased slightly to 183.93 mg/g once the agitation time reached 30 min. Consequently, an agitation time of 20 min was chosen to be the perfect time for subsequent examinations. Generally, at the beginning of the adsorption process, numerous vacant sites of adsorbent are vacant to interact with *amoxicillin* molecules in solution. The functional group's interaction of the adsorbent and the *amoxicillin* grow stronger once the agitation time is increased to 20 min. At longer time frames (>20 min), there was no more improvement in Q_e , which was probably related to the existence of adsorbent active sites and the equilibrium state approach.

Amoxicillin initial concentration: The association between the *amoxicillin* initial concentration and the Q_e of the CMT-g-PANI@ Fe_2O_3 adsorbent was studied by altering the *amoxicillin* concentration from 50 to 400 mg/L at the optimal pH (7.0), dose (0.005 g), and agitation time (20 min). Figure 6D shows that the *amoxicillin* initial concentration influences the Q_e of CMT-g-PANI@ Fe_2O_3 adsorbent. With increasing the *amoxicillin* initial concentration from 50 to 400 mg/L, Q_e of adsorbent with an intensity rose to 788.83 mg/g with a steep slope. Thus, the Q_e increases once the *amoxicillin* initial concentration is increased, whereas the adsorbent amount remains constant, and this pattern holds until the *amoxicillin* initial concentration reaches an equilibrium level.

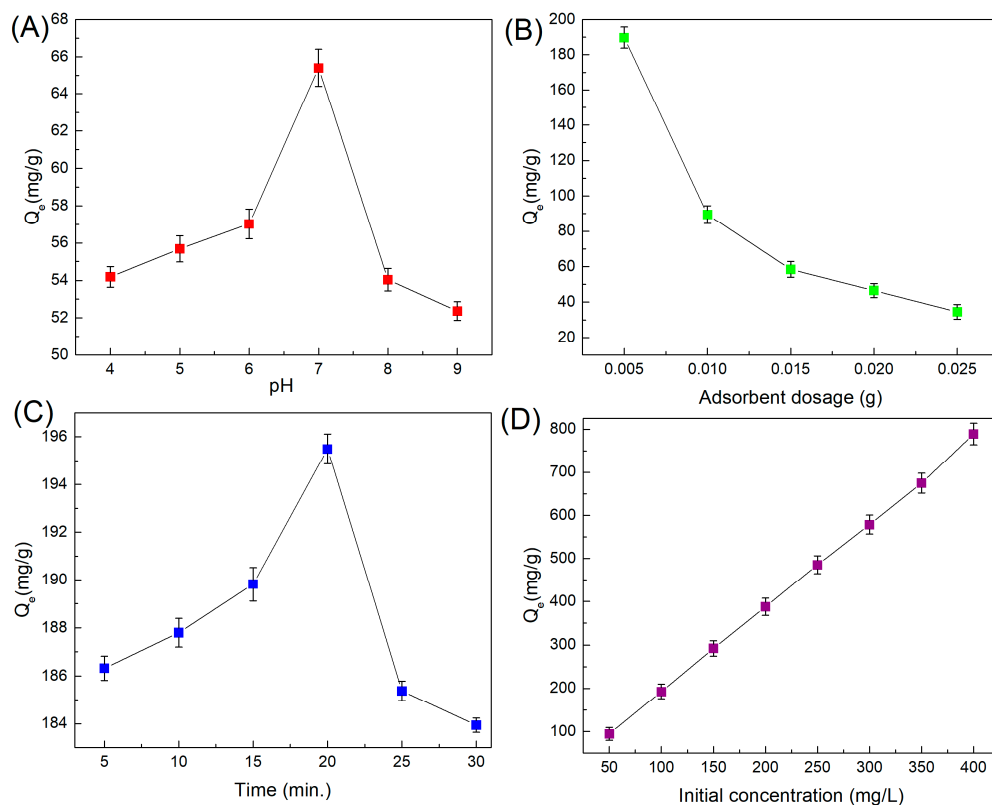


Figure 6. (A) Effect of pH (4–9), (biosorbent dose = 0.015 g, amoxicillin concentration = 100 mg/L, time = 15 min and temperature = 298 K), (B) biosorbent dosage (0.005–0.025 g), (pH 7, amoxicillin concentration = 100 mg/L, time = 15 min and temperature = 298 K), (C) time (5–30 min), (pH 7, biosorbent dosage = 0.005 g, amoxicillin concentration = 100 mg/L, $V = 10$ mL, and temperature = 298 K), (D) amoxicillin concentration (50–400 mg/L), (pH 7, biosorbent dosage = 0.005 g, $V = 10$ mL, time = 20 min, temperature = 298 K).

3.3. Adsorption Isotherm

To find the interaction between amoxicillin and CMT-g-PANI@Fe₂O₃ bioadsorbent, the isotherm study was employed. It is well known that Langmuir and Freundlich's isotherm models are used to evaluate the maximum adsorption capacity and equilibrium adsorption isotherms. Figure 7A,B demonstrates the Langmuir and Freundlich isotherm. The obtained parameters of isotherm models are tabulated in Table 2. Consistent with obtained correlation coefficient (R^2) of isotherm models, the Freundlich isotherm was found to be more reliable with the experimental data than the Langmuir model. This result shows that the amoxicillin adsorbed over the CMT-g-PANI@Fe₂O₃ bioadsorbent surface as a multilayer. In addition, the obtained "n" in the Freundlich model is an important parameter to define the adsorption process favorability. The value of $n > 1$ in Table 2 shows that the amoxicillin adsorbed over the CMT-g-PANI@Fe₂O₃ bioadsorbent surface is desirable at high concentrations.

The comparison of Q_{max} for amoxicillin to other adsorbents reported in recent years showed that the CMT-g-PANI@Fe₂O₃ biosorbent has a higher maximum adsorption capacity (909.09 mg·g) than other adsorbents (Table 3). This could be related to the presence of Fe₂O₃ nanoparticles and numerous active sites, for example, hydroxyl, carboxylate, and amine groups in the nanocomposite, which can effectively interact with amoxicillin (via electrostatic interaction and hydrogen bonding), led to eliminating the amoxicillin.

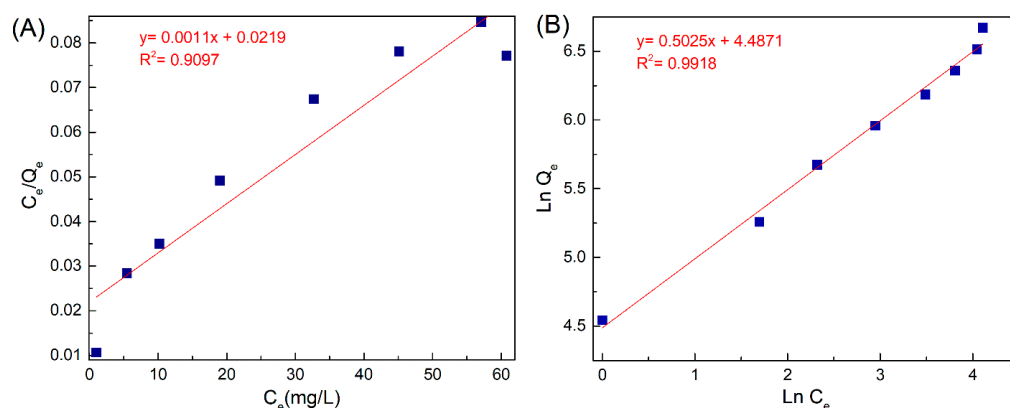


Figure 7. (A) Langmuir and (B) Freundlich isotherms (condition: amoxicillin concentration (50–400 mg/L), pH 7, biosorbent dosage = 0.005 g, contact time = 20 min, T = 298 K).

Table 2. Isotherm parameters, for amoxicillin adsorption onto the CMT-g-PANI@Fe₂O₃ bioadsorbent.

Isotherm	Parameters	
Freundlich	K _F	88.8633
	n	1.99
	R ²	0.9918
Langmuir	Q _{max}	909.09
	K _L	0.0502
	R ²	0.9097

Table 3. Assessment of the maximum adsorption capacity of CMT-g-PANI@Fe₂O₃ bionanocomposite with other reported studies.

Adsorbent	Experimental Conditions	Q _{max} (mg/g)	Ref.
MIL-53(Al) metal-organic framework	pH: 7.5, adsorbent dosage: 0.1 g/L, contact time: 12 h, T: 303 K, initial concentration: 50 mg/L	758.5	[22]
NH ₄ Cl-induced activated carbon	pH: 6, adsorbent dosage: 0.8 g/L, contact time: 30 min, T: 303 K, initial concentration: 100 mg/L	437	[23]
Activated carbon/iron nanoparticles	pH: 5, adsorbent dosage: 1.5 g/L, contact time: 30 min, T: 298 K, initial concentration: 10 mg/L	40.282	[24]
Functional CoFe ₂ O ₄ -modified biochar	pH: 7, adsorbent dosage: 0.05 g/L, contact time: 60 min, T: 298 K, initial concentration: 50 mg/L	99.99	[25]
Activated carbon	pH: 5.5, adsorbent dosage: 0.06 g/L, contact time: 240, T: 298 K, initial concentration: 100 mg/L	4.4	[42]
Mg-Al layered double hydroxide/cellulose nanocomposite	pH: 7, adsorbent dosage: 0.1 g/L, contact time: 20 min, T: 298 K, initial concentration: 120 mg/L	138.3	[43]
Concrete-based hydrotalcite	pH: 5, adsorbent dosage: 0.1 g/L, contact time: 12 h, T: 298 K, initial concentration: 400 mg/L	49.7	[44]
Chitosan-coated Fe ₃ O ₄ @Cd-MOF microspheres	pH: 8, adsorbent dosage: 0.05 g/L, contact time: 240 min, T: 298 K, initial concentration: 50 mg/L	103.09	[45]
Fe ₃ O ₄ /SiO ₂ /CTAB-SiO ₂	pH: 5, adsorbent dosage: 0.009 g/L, contact time: 60 min, T: 298 K, initial concentration: 25 mg/L	362.66	[46]
Fe ₃ O ₄ @activated carbon	pH: 6, adsorbent dosage: 0.5 g/L, contact time: 90 min, T: 298 K, initial concentration: 200 mg/L	238.1	[47]
CMT-g-PANI@Fe ₂ O ₃	pH: 7, adsorbent dosage: 0.005 g/L, contact time: 20 min, T: 298 K, initial concentration: 400 mg/L	909.09	Current work

3.4. Adsorption Kinetic

For discovering and evaluating possible adsorption routes, equilibrium time, and adsorption rate-limiting phase of amoxicillin adsorbed over the CMT-g-PANI@Fe₂O₃ adsorbent used the PFO and PSO kinetics models. In addition, kinetic models are employed to define the adsorption process mechanism, for example, surface and chemical adsorption. The PFO is based on the adsorbent capacity and employed once adsorption happens via diffusion in a border layer, whereas the PSO expresses that the chemical adsorption procedure is the main controlling procedure. Figure 8A,B and Table 4 exhibit kinetic linear plots, and their calculated parameters. According to R², the difference between the estimated Q_e and observed Q_e values, the PSO is more appropriate for considering the amoxicillin adsorption kinetics on the CMT-g-PANI@Fe₂O₃. Consequently, chemical adsorption is the main mechanism in the adsorption of amoxicillin on the adsorbent and it displays that, in addition to amoxicillin molecules, the CMT-g-PANI@Fe₂O₃ adsorbent is involved in the adsorption procedure.

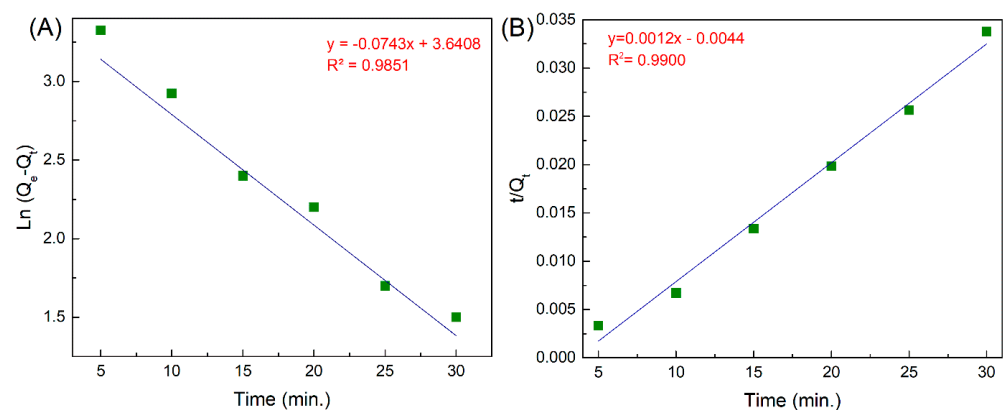


Figure 8. (A) Pseudo-first-order and (B) pseudo-second-order models (Contact time (5–30 min), pH 7, biosorbent dosage = 0.005 g, amoxicillin concentration = 400 mg/L, T = 298 K).

Table 4. Kinetic parameters, for amoxicillin adsorption on the CMT-g-PANI@Fe₂O₃.

Models	Parameters	
Pseudo-first-order	k ₁	0.0743
	Q _e calculated	38.122
	Q _e experimental	788.73
	R ²	0.9851
Pseudo-second-order	k ₂	0.000001
	Q _e	833.33
	Q _e experimental	788.83
	R ²	0.9900

3.5. Desorption and Reusability

The reusability of adsorbent is a significant factor to create the adsorption procedure economically. The reusability of adsorbent can be effective for its use in numerous consecutive cycles without considerable performance debility. In the present work, we evaluated the amoxicillin desorption and reusability of CMT-g-PANI@Fe₂O₃ bioadsorbent in three consecutive cycles, and an ethanolic solution was investigated. In this regard, amoxicillin adsorbed onto the CMT-g-PANI@Fe₂O₃ was performed in optimal conditions and was immersed into ethanol (10 mL) under stirring at room temperature for 1 h to desorb amoxicillin. Afterward, CMT-g-PANI@Fe₂O₃ was collected by a magnet, washed with distilled water, and then dried for successive adsorption/desorption processes. Then, the released amoxicillin amount in the elution medium was measured using a UV-visible spectrophotometer. Figure 9 demonstrates that the adsorption percentage decreased from

98.59 % to 94.03%, and the desorption percentage decreased from 94.41% to 92.001% after three consecutive cycles, these results show that the CMT-g-PANI@Fe₂O₃ could continue to remove *amoxicillin* after three consecutive cycles of adsorption/desorption process without considerably losing adsorption capacity.

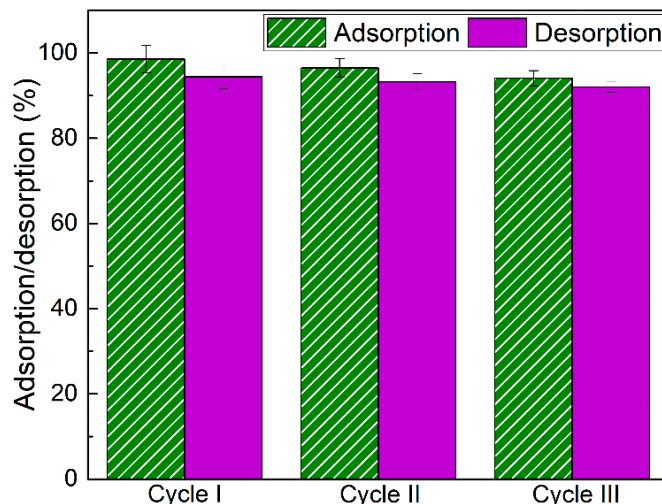


Figure 9. Desorption and reusability of the CMT-g-PANI@Fe₂O₃ bioadsorbent for *amoxicillin* adsorption.

3.6. Suggested Mechanism of Amoxicillin Adsorption

The pollutant adsorption mechanism by the adsorbent depends on the functional groups and morphology of the adsorbent, which can be created a synergistic effect in increasing the pollutant adsorption by the adsorbent. Considering that the CMT-g-PANI@Fe₂O₃ bioadsorbent has amine, carboxylate, and hydroxyl functional groups, it can create intermolecular interactions such as hydrogen bonding, electrostatic and π - π interactions with the *amoxicillin* antibiotic, and cause its efficient adsorption on the CMT-g-PANI@Fe₂O₃ bioadsorbent as shown in Figure 10.

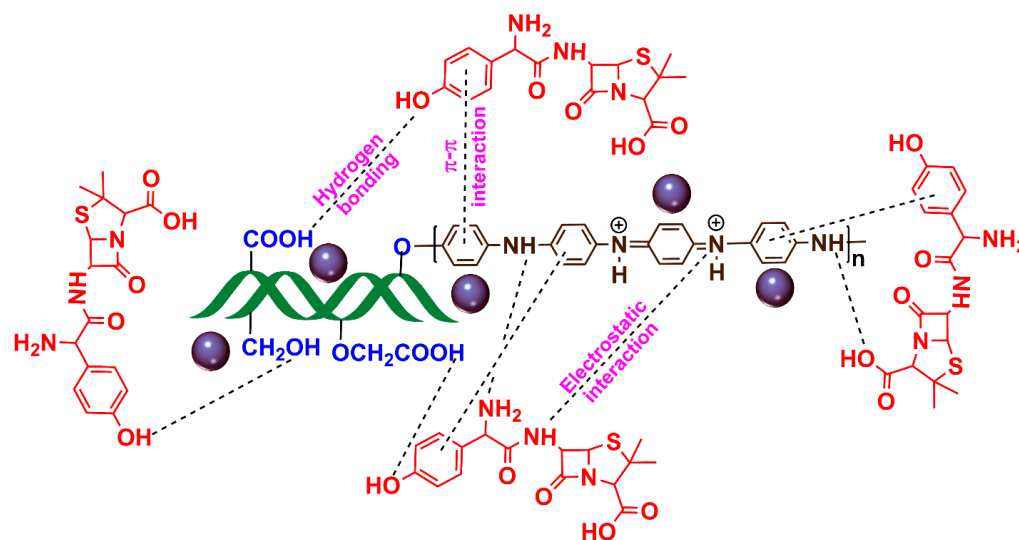


Figure 10. A schematic of the suggested mechanism of *amoxicillin* adsorption by CMT-g-PANI@Fe₂O₃ bioadsorbent.

4. Conclusions

A magnetic bionanocomposite was synthesized by an in situ copolymerization method from carboxy methyl tragacanth gum in the presence of aniline monomer and γ Fe₂O₃ nanoparticles (CMT-g-PANI@Fe₂O₃). The CMT-g-PANI@Fe₂O₃ bionanocomposite was

characterized by several analyses and employed as a bioadsorbent for the removal of *amoxicillin* antibiotic from contaminated water. A granular structure with good thermal stability (char yield 34 wt%), magnetization saturation (25 emu g⁻¹), and a specific surface area (8.0794 m²/g) observed for CMT-g-PANI@Fe₂O₃ bionanocomposite. The maximum adsorption capacity (909.09 mg/g) was found at pH 7, an agitation time of 20 min, an adsorbent dose of 0.005 g, and an *amoxicillin* initial concentration of 400 mg/L. The Freundlich isotherm and pseudo-second-order kinetic models fit closely with the experimental data. The adsorption/desorption process showed that the CMT-g-PANI@Fe₂O₃ could continue to remove *amoxicillin* after three consecutive cycles without considerably losing adsorption capacity. The intermolecular interactions such as hydrogen bonding, electrostatic, and π - π interactions between *amoxicillin* antibiotic and CMT-g-PANI@Fe₂O₃ were suggested for the adsorption mechanism of *amoxicillin* antibiotic by bionanocomposite.

Author Contributions: Conceptualization, E.N.Z.; methodology, S.S.M.; software, E.N.Z.; validation, E.N.Z., H.B. and M.T.; formal analysis, S.S.M.; investigation, E.N.Z., H.B. and M.T.; data curation, S.S.M.; writing—original draft preparation, E.N.Z.; writing—review and editing, E.N.Z., H.B. and M.T.; supervision, E.N.Z., H.B. and M.T.; project administration E.N.Z.; funding acquisition, S.S.M. All authors have read and agreed to the published version of the manuscript.

Funding: This research received no external funding.

Data Availability Statement: Data is available upon request.

Acknowledgments: The authors are grateful for the support of Damghan University's financial support.

Conflicts of Interest: The authors declare no conflict of interest.

References

1. Ahmadi, S.A.R.; Kalae, M.R.; Moradi, O.; Nosratinia, F.; Abdouss, M. Core-shell activated carbon-ZIF-8 nanomaterials for the removal of tetracycline from polluted aqueous solution. *Adv. Compos. Hybrid. Mater.* **2021**, *4*, 1384–1397. [[CrossRef](#)]
2. Li, Z.; Xie, W.; Yao, F.; Du, A.; Wang, Q.; Guo, Z.; Gu, H. Comprehensive electrocatalytic degradation of tetracycline in wastewater by electrospun perovskite manganite nanoparticles supported on carbon nanofibers. *Adv. Compos. Hybrid. Mater.* **2022**, *5*, 2092–2105. [[CrossRef](#)]
3. Zare, E.N.; Fallah, Z.; Le, V.T.; Doan, V.D.; Mudhoo, A.; Joo, S.W.; Vasseghian, Y.; Tajbakhsh, M.; Moradi, O.; Sillanpää, M.; et al. Remediation of pharmaceuticals from contaminated water by molecularly imprinted polymers: A review. *Environ. Chem. Lett.* **2022**, *20*, 2629–2664. [[CrossRef](#)] [[PubMed](#)]
4. Limousy, L.; Ghouma, I.; Ouederni, A.; Jeguirim, M. Amoxicillin removal from aqueous solution using activated carbon prepared by chemical activation of olive stone. *Environ. Sci. Pollut. Res.* **2017**, *24*, 9993–10004. [[CrossRef](#)] [[PubMed](#)]
5. Naeini, A.H.; Kalae, M.R.; Moradi, O.; Khajavi, R.; Abdouss, M. Synthesis, characterization and application of Carboxymethyl cellulose, Guar gum, and Graphene oxide as novel composite adsorbents for removal of malachite green from aqueous solution. *Adv. Compos. Hybrid. Mater.* **2022**, *5*, 335–349. [[CrossRef](#)]
6. Zhu, J.; Tian, M.; Zhang, Y.; Zhang, H.; Liu, J. Fabrication of a novel “loose” nanofiltration membrane by facile blending with Chitosan–Montmorillonite nanosheets for dyes purification. *Chem. Eng. J.* **2015**, *265*, 184–193. [[CrossRef](#)]
7. Bebu, A.; Szabó, L.; Leopold, N.; Berindean, C.; David, L. IR, Raman, SERS and DFT study of amoxicillin. *J. Mol. Struct.* **2011**, *993*, 52–56. [[CrossRef](#)]
8. Andreozzi, R.; Canterino, M.; Marotta, R.; Paxeus, N. Antibiotic removal from wastewaters: The ozonation of amoxicillin. *J. Hazard. Mater.* **2005**, *122*, 243–250. [[CrossRef](#)]
9. Sánchez-Montes, I.; Fuzer Neto, J.R.; Silva, B.F.; Silva, A.J.; Aquino, J.M.; Rocha-Filho, R.C. Evolution of the antibacterial activity and oxidation intermediates during the electrochemical degradation of norfloxacin in a flow cell with a PTFE-doped β -PbO₂ anode: Critical comparison to a BDD anode. *Electrochim. Acta* **2018**, *284*, 260–270. [[CrossRef](#)]
10. Ioannou-Ttofa, L.; Raj, S.; Prakash, H.; Fatta-Kassinos, D. Solar photo-Fenton oxidation for the removal of ampicillin, total cultivable and resistant *E. coli* and ecotoxicity from secondary-treated wastewater effluents. *Chem. Eng. J.* **2019**, *355*, 91–102. [[CrossRef](#)]
11. Rodríguez-Chueca, J.; Della Giustina, S.V.; Rocha, J.; Fernandes, T.; Pablos, C.; Encinas, Á.; Barceló, D.; Rodríguez-Mozaz, S.; Manaia, C.M.; Marugán, J. Assessment of full-scale tertiary wastewater treatment by UV-C based-AOPs: Removal or persistence of antibiotics and antibiotic resistance genes? *Sci. Total Environ.* **2019**, *652*, 1051–1061. [[CrossRef](#)] [[PubMed](#)]
12. Alizadeh, E.; Baseri, H. Photocatalytic degradation of Sumatriptan Succinate by ZnO, Fe doped ZnO and TiO₂-ZnO nanocatalysts. *Mater. Chem. Horizons* **2022**, *1*, 7–21. [[CrossRef](#)]
13. Alsager, O.A.; Alnajrani, M.N.; Abuelizz, H.A.; Aldaghmani, I.A. Removal of antibiotics from water and waste milk by ozonation: Kinetics, byproducts, and antimicrobial activity. *Ecotoxicol. Environ. Saf.* **2018**, *158*, 114–122. [[CrossRef](#)]

14. Cheng, D.; Ngo, H.H.; Guo, W.; Liu, Y.; Chang, S.W.; Nguyen, D.D.; Nghiem, L.D.; Zhou, J.; Ni, B. Anaerobic membrane bioreactors for antibiotic wastewater treatment: Performance and membrane fouling issues. *Bioresour. Technol.* **2018**, *267*, 714–724. [[CrossRef](#)] [[PubMed](#)]
15. Ghanbari, R.; Amanat, N. Approaches of Membrane Modification for Water Treatment. *Mater. Chem. Horizons.* **2022**, *1*, 153–167. [[CrossRef](#)]
16. Neghi, N.; Krishnan, N.R.; Kumar, M. Analysis of metronidazole removal and micro-toxicity in photolytic systems: Effects of persulfate dosage, anions and reactor operation-mode. *J. Environ. Chem. Eng.* **2018**, *6*, 754–761. [[CrossRef](#)]
17. Tiwari, B.; Sellamuthu, B.; Ouarda, Y.; Drogui, P.; Tyagi, R.D.; Buelna, G. Review on fate and mechanism of removal of pharmaceutical pollutants from wastewater using biological approach. *Bioresour. Technol.* **2017**, *224*, 1–12. [[CrossRef](#)]
18. Nasseh, N.; Barikbin, B.; Taghavi, L.; Nasser, M.A. Adsorption of metronidazole antibiotic using a new magnetic nanocomposite from simulated wastewater (isotherm, kinetic and thermodynamic studies). *Compos. Part B Eng.* **2019**, *159*, 146–156. [[CrossRef](#)]
19. Movagharneshad, N.; Ehsanimehr, S.; Najafi Moghadam, P. Synthesis of Poly (N-vinylpyrrolidone)-grafted-Magnetite Bromoacetylated Cellulose via ATRP for Drug Delivery. *Mater. Chem. Horizons.* **2022**, *1*, 89–98. [[CrossRef](#)]
20. Mehdizadeh, A.; Najafi Moghadam, P.; Ehsanimehr, S.; Fareghi, A.R. Preparation of a New Magnetic Nanocomposite for the Removal of Dye Pollutions from Aqueous Solutions: Synthesis and Characterization. *Mater. Chem. Horizons.* **2022**, *1*, 23–34. [[CrossRef](#)]
21. Akter, T.; Bañuelos, J.L.; Andrade, D.; Bañuelos, D.I.; Saupe, G.B. Rapid Adsorption Mechanism of Methylene Blue onto a Porous Mixed Ti-Nb Oxide. *Mater. Chem. Horizons.* **2022**, *1*, 49–67. [[CrossRef](#)]
22. Imanipoor, J.; Mohammadi, M.; Dinari, M.; Ehsani, M.R. Adsorption and desorption of amoxicillin antibiotic from water matrices using an effective and recyclable MIL-53 (Al) metal-organic framework adsorbent. *J. Chem. Eng. Data* **2020**, *66*, 389–403. [[CrossRef](#)]
23. Moussavi, G.; Alahabadi, A.; Yaghmaeian, K.; Eskandari, M. Preparation, characterization and adsorption potential of the NH₄Cl-induced activated carbon for the removal of amoxicillin antibiotic from water. *Chem. Eng. J.* **2013**, *217*, 119–128. [[CrossRef](#)]
24. Ali, I.; Afshinb, S.; Poureshgh, Y.; Azari, A.; Rashtbari, Y.; Feizizadeh, A.; Hamzezadeh, A.; Fazlzadeh, M. Green preparation of activated carbon from pomegranate peel coated with zero-valent iron nanoparticles (nZVI) and isotherm and kinetic studies of amoxicillin removal in water. *Environ. Sci. Pollut. Res.* **2020**, *27*, 36732–36743. [[CrossRef](#)]
25. Chakhtouna, H.; Benzeid, H.; Zari, N.; Bouhfid, R. Functional CoFe₂O₄-modified biochar derived from banana pseudostem as an efficient adsorbent for the removal of amoxicillin from water. *Sep. Purif. Technol.* **2021**, *266*, 118592. [[CrossRef](#)]
26. Taghavizadeh Yazdi, M.E.; Nazarnezhad, S.; Mousavi, S.H.; Sadegh Amiri, M.; Darroudi, M.; Baino, F.; Kargozar, S. Gum Tragacanth (GT): A Versatile Biocompatible Material beyond Borders. *Molecules* **2021**, *26*, 1510. [[CrossRef](#)] [[PubMed](#)]
27. Verbeken, D.; Dierckx, S.; Dewettinck, K. Exudate gums: Occurrence, production, and applications. *Appl. Microbiol. Biotechnol.* **2003**, *63*, 10–21. [[CrossRef](#)] [[PubMed](#)]
28. Tischer, C.A.; Iacomini, M.; Gorin, P.A.J. Structure of the arabinogalactan from gum tragacanth (*Astragalus gummifer*). *Carbohydr. Res.* **2002**, *337*, 1647–1655. [[CrossRef](#)] [[PubMed](#)]
29. Nejatian, M.; Abbasi, S.; Azarikia, F. Gum Tragacanth: Structure, characteristics and applications in foods. *Int. J. Biol. Macromol.* **2020**, *160*, 846–860. [[CrossRef](#)]
30. Zare, E.N.; Makvandi, P.; Tay, F.R. Recent progress in the industrial and biomedical applications of tragacanth gum: A review. *Carbohydr. Polym.* **2019**, *212*, 450–467. [[CrossRef](#)]
31. Abdollahi, Z.; Zare, E.N.; Salimi, F.; Goudarzi, I.; Tay, F.R.; Makvandi, P. Bioactive carboxymethyl starch-based hydrogels decorated with cuo nanoparticles: Antioxidant and antimicrobial properties and accelerated wound healing in vivo. *Int. J. Mol. Sci.* **2021**, *22*, 2531. [[CrossRef](#)] [[PubMed](#)]
32. Sudhakara, K.; Kumar, A.P.; Kumara, B.P.; Raghavendera, A.; Ravia, S.; Kenie, D.N.; Lee, Y.I. Synthesis of γ -Fe₂O₃ nanoparticles and catalytic activity of azide-alkyne cycloaddition reactions. *Asian J. Nanosci. Mater.* **2018**, *1*, 172–182.
33. Hassanzadeh-Afruzi, F.; Heidari, G.; Maleki, A. Magnetic Nanocomposite Hydrogel based on Arabic Gum for Remediation of Lead(II) from Contaminated Water. *Mater. Chem. Horizons.* **2022**, *1*, 107–122. [[CrossRef](#)]
34. Behrouzi, M.; Moghadam, P.N. Synthesis of a new superabsorbent copolymer based on acrylic acid grafted onto carboxymethyl tragacanth. *Carbohydr. Polym.* **2018**, *202*, 227–235. [[CrossRef](#)] [[PubMed](#)]
35. Janani, N.; Zare, E.N.; Salimi, F.; Makvandi, P. Antibacterial tragacanth gum-based nanocomposite films carrying ascorbic acid antioxidant for bioactive food packaging. *Carbohydr. Polym.* **2020**, *247*, 116678. [[CrossRef](#)]
36. Long, Z.; Yuan, L.; Shi, C.; Wu, C.; Qiao, H.; Wang, K. Porous Fe₂O₃ nanorod-decorated hollow carbon nanofibers for high-rate lithium storage. *Adv. Compos. Hybrid. Mater.* **2022**, *5*, 370–382. [[CrossRef](#)]
37. Yan, Z.; Sun, Z.; Li, A.; Liu, H.; Guo, Z.; Qian, L. Three-dimensional porous flower-like S-doped Fe₂O₃ for superior lithium storage. *Adv. Compos. Hybrid. Mater.* **2021**, *4*, 716–724. [[CrossRef](#)]
38. Shao, W.; Jamal, R.; Xu, F.; Ubul, A.; Abdiryim, T. The effect of a small amount of water on the structure and electrochemical properties of solid-state synthesized polyaniline. *Materials* **2012**, *5*, 1811–1825. [[CrossRef](#)]
39. Bachra, Y.; Grouli, A.; Damiri, F.; Talbi, M.; Berrada, M. A Novel Superabsorbent Polymer from Crosslinked Carboxymethyl Tragacanth Gum with Glutaraldehyde: Synthesis, Characterization, and Swelling Properties. *Int. J. Biomater.* **2021**, *2021*, 5008833. [[CrossRef](#)]
40. Ganachari, S.V.; Joshi, V.K.; Bhat, R.; Deshpande, R.; Salimath, B.; Rao, N. V Large scale synthesis and characterization of γ -Fe₂O₃ nanoparticles by self-propagating low temperature combustion method. *Int. J. Sci. Res.* **2012**, *1*, 77–79.

41. Van Cuong, N.; Hieu, T.Q.; Thien, P.T.; Vu, L.D.; Van Tan, L. Reusable starch-graft-polyaniline/Fe₃O₄ composite for removal of textile dyes. *Rasayan J. Chem.* **2017**, *10*, 1446–1454. [[CrossRef](#)]
42. de Franco, M.A.E.; de Carvalho, C.B.; Bonetto, M.M.; de Pelegrini Soares, R.; Féris, L.A. Removal of amoxicillin from water by adsorption onto activated carbon in batch process and fixed bed column: Kinetics, isotherms, experimental design and breakthrough curves modelling. *J. Clean. Prod.* **2017**, *161*, 947–956. [[CrossRef](#)]
43. Yang, C.; Wang, L.; Yu, Y.; Wu, P.; Wang, F.; Liu, S.; Luo, X. Highly efficient removal of amoxicillin from water by Mg-Al layered double hydroxide/cellulose nanocomposite beads synthesized through in-situ coprecipitation method. *Int. J. Biol. Macromol.* **2020**, *149*, 93–100. [[CrossRef](#)]
44. Liu, X.; Yang, S.; Feng, T.; Zhong, H.; Cao, S.; Chen, Y. Removal of amoxicillin from water by concrete-based hydrotalcites: Efficiency and mechanism. *Process Saf. Environ. Prot.* **2022**, *163*, 210–217. [[CrossRef](#)]
45. Pooresmaeil, M.; Namazi, H. Chitosan coated Fe₃O₄@Cd-MOF microspheres as an effective adsorbent for the removal of the amoxicillin from aqueous solution. *Int. J. Biol. Macromol.* **2021**, *191*, 108–117. [[CrossRef](#)] [[PubMed](#)]
46. Zandipak, R.; Sobhanardakani, S. Novel mesoporous Fe₃O₄/SiO₂/CTAB-SiO₂ as an effective adsorbent for the removal of amoxicillin and tetracycline from water. *Clean Technol. Environ. Policy* **2018**, *20*, 871–885. [[CrossRef](#)]
47. Jafari, K.; Heidari, M.; Rahmadian, O. Wastewater treatment for Amoxicillin removal using magnetic adsorbent synthesized by ultrasound process. *Ultrason. Sonochem.* **2018**, *45*, 248–256. [[CrossRef](#)]

Disclaimer/Publisher’s Note: The statements, opinions and data contained in all publications are solely those of the individual author(s) and contributor(s) and not of MDPI and/or the editor(s). MDPI and/or the editor(s) disclaim responsibility for any injury to people or property resulting from any ideas, methods, instructions or products referred to in the content.